Journal of CO2 Utilization 97 (2025) 103119

Contents lists available at ScienceDirect

Journal of CO2 Utilization

journal homepage: www.elsevier.com/locate/jcou

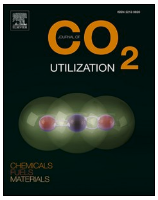

Nickel mobilization during single-stage aqueous mineral carbonation of serpentinized peridotite at 185 °C and P_{CO_2} of 100 bar

Błażej Cieślik [a,*], Alicja Lacinska [b], Anna Pietranik [a], Maciej Róziewicz [c], Artur Pędziwiatr [d], Krzysztof Turniak [a], Agata Łamacz [c], Jakub Kierczak [a]

[a] *University of Wrocław, Institute of Geological Sciences, Pl. M. Borna 9, Wrocław 50-204, Poland*
[b] *British Geological Survey, Natural Environment Research Council, Environmental Science Centre, Keyworth, Nottingham NG12 5GG, United Kingdom*
[c] *Department of Engineering and Technology of Chemical Processes, Wroclaw University of Science and Technology, Wrocław, Poland*
[d] *Institute of Agriculture, Warsaw University of Life Sciences WULS-SGGW, ul. Nowoursynowska 159, b.37, Warsaw 02-787, Poland*

ARTICLE INFO

Keywords:
Single-stage mineral carbonation
Nickel mobilization
Serpentinized peridotite
Forsterite dissolution

ABSTRACT

Forsterite-rich ultramafic rocks, such as serpentinized peridotites, are considered highly promising natural materials for mineral carbonation – a carbon capture and storage (CCS) technique aimed at reducing atmospheric carbon dioxide (CO_2) by sequestering carbon as carbonate minerals. These rocks are commonly characterized by a high content of divalent cations, including nickel (Ni^{2+}), whose behavior and mobility during mineral carbonation remain insufficiently understood. This issue is critical, as the large-scale application of mineral carbonation may pose ecotoxicological risks by mobilizing specific metallic elements naturally occurring in ultramafic rocks. To elucidate possible Ni mobility during single-stage aqueous mineral carbonation, 15 g of powdered serpentinized peridotite was carbonated in a batch-type reactor for 96 hours at 185°C and a P_{CO_2} of 100 bar. The experiment resulted in the dissolution of forsterite and the extensive crystallization of magnesite, demonstrating that the serpentinized peridotite is a highly effective natural material for permanent CO_2 storage in the single-stage carbonation processes. Nickel released during the dissolution of forsterite (approximately 50 % of the whole Ni budget) was mainly incorporated in newly formed Ni-rich phyllosilicates (more than 98 %) and a small portion was mobilized into the post-carbonation fluid (less than 2 %), reaching a concentration of approximately18 mg/kg after 96 hours. The presence of Ni in newly crystallized magnesite crystals has not been detected. These results suggest that the behavior of Ni during single-stage mineral carbonation is complex and requires careful monitoring to prevent potential negative impacts on the natural environment.

1. Introduction

Modern global climate change is attributed to the intensification of the greenhouse effect, primarily driven by anthropogenic carbon dioxide (CO_2) emissions. Atmospheric CO_2 concentrations have steadily risen, surpassing 427 ppm at the beginning of 2025, compared to approximately 300 ppm in 1960 [1,2]. In recent decades, substantial progress has been made in developing a wide range of carbon capture and storage (CCS) techniques and strategies utilizing rocks and minerals [3–8]. One promising technology that aims for long-term and stable CO_2 removal is single-stage mineral carbonation, which involves the carbonation of natural (rocks and minerals) and anthropogenic (e.g, alkaline industrial wastes) materials in a single reactor under high-pressure (up to 180 bar) and high-temperature (up to 185°C) conditions [9–12]. The process of mineral dissolution in a CO_2-rich aqueous solution generates unbound cations, which subsequently interact with carbonate ions (CO_3^{2-}), resulting in the formation of carbonates. The divalent metals, specifically magnesium (Mg^{2+}), calcium (Ca^{2+}), and iron (Fe^{2+}), are the most reactive ions, and their natural source are mafic and ultramafic igneous rocks [13–15].

Peridotites, the main representative of the ultramafic rocks group, predominantly comprise Mg-rich silicates, such as olivine and clino- and orthopyroxene. When exposed to water, peridotites can undergo reactions that form hydrous Mg-phyllosilicates, known as serpentines [16]. The abundance of various Mg-rich silicates in peridotites makes these rocks attractive for studies exploring their potential as a feedstock for mineral carbonation. Despite a few unique field projects enabling direct CO_2 injection into geological formation (in situ), the primary

---

* Corresponding author.
E-mail address: blazej.cieslik2@uwr.edu.pl (B. Cieślik).

https://doi.org/10.1016/j.jcou.2025.103119
Received 23 January 2025; Received in revised form 6 May 2025; Accepted 12 May 2025

understanding of mineral carbonation in ultramafic rocks comes from laboratory-scale studies or industrial pilot projects that utilize mining wastes (ex situ) [7,14,17–23].

While serpentinized peridotites are characterized by significant Mg content, which is beneficial to mineral carbonation, they also exhibit elevated Ni concentrations. Whole rock analyses of a large number of ultramafic rocks from various environments show that Ni concentrations in these rocks can reach 10000 mg/kg [24,25]. In contrast, mafic rocks like basalts, which are also recognized as a promising feedstock for mineral carbonation, have an average Ni content of 200 mg/kg [7,26]. The majority of Ni in peridotites is predominantly hosted in forsterite, the Mg-rich end-member of the olivine solid solution series, $(Mg,Fe)_2SiO_4$. In the forsterite structure, Ni^{2+} typically substitutes for Mg^{2+} within the crystal lattice [27]. Ni is also present in Fe-Ni sulfides (e.g. pentlandite) and spinel-group minerals, which commonly occur as accessory phases in most ultramafic rocks.

Few studies have investigated the fate of trace metals and their impact on the safety of CO_2 storage during ex situ mineral carbonation. These studies can generally be categorized into two main areas. One focuses mostly on the mobility of metals, highlighting it as an environmental concern. For example, it was demonstrated that some trace metals, including Ni, could be captured by synthetic Mg carbonates, such as nesquehonite ($MgCO_3{\cdot}3H_2O$) [28]. However, in this experiment, trace metals were introduced to the reactor as hydrated divalent metal chloride salts rather than being supplied through the dissolution of natural magnesium silicates. Trace metals mobilization has been observed during passive mineral carbonation of ultramafic mine tailings in New South Wales, Australia [29]. It has been shown that cations of iron and trace metals (Cr, Ni, Mn, Co) are immobilized within naturally formed hydromagnesite $[Mg_5(CO_3)_4(OH)_2{\cdot}4H_2O]$ cements. Chemical analysis of the mine pit waters from the same locality revealed that first-row transition metals concentrations are below instrumental detection limits. The deterioration of Ni-bearing minerals drives Ni mobilization, posing significant risks to biological life [30]. The World Health Organization (WHO) guidelines, updated in 2021, set drinking water's maximum permissible Ni content at 0.07 mg/L [31]. Additionally, it has been observed that organisms consuming water with Ni concentrations above this threshold are at risk of various health complications [32].

The second group of studies explores strategies for metal recovery as a process that may accompany ex situ mineral carbonation. For example, Santos et al. [33] investigated the potential for Ni recovery through mineral carbonation. The results showed that inorganic acids successfully leached 91–100 % of Ni from carbonated olivine. In contrast, only 64–66 % of Ni was leached out from uncarbonated olivine under identical conditions. Wang and Dreisinger [34] demonstrated that Ni extraction efficiencies of up to 90 % can be achieved during ex situ carbonation of natural olivine, along with a CO_2 mineralization efficiency exceeding 50 %. Furthermore, additional Ni recovery can be accomplished through sulfide precipitation. A recent study has indicated that mineral carbonation of serpentinite may serve as a pretreatment, as the carbonation process converts serpentines into magnesite and silica, altering the anisotropic surface charge. This alteration enhances the froth flotation of Ni-bearing pentlandite from low-grade ultramafic Ni ore (containing < 1 % Ni in pentlandite) [35].

Given the limited knowledge of Ni behavior during mineral carbonation, we conducted a single-stage mineral carbonation experiment using serpentinized peridotite. This rock contains the main Mg-rich phases commonly found in ultramafic rocks, such as forsterite and serpentines, but also Fe-Cr spinels, amphiboles, and sulfides. These phases may be carbonated at different rates and release Ni to the system. Our study aims to understand the behavior of Ni^{2+} cations during single-stage aqueous mineral carbonation. This knowledge is essential for evaluating the potential environmental risks associated with large-scale ex situ carbonation projects using ultramafic rocks. Specifically, it aims to determine whether Ni is released into carbonating fluids or incorporated into solid products of mineral carbonation.

2. Material and methods

2.1. Source of experimental material

As a feedstock for the single-stage carbonation experiment, we used serpentinized peridotite sourced from the mafic-ultramafic Braszowice-Brzeźnica Massif (BBM), part of the Central Sudetic Ophiolite (CSO). The CSO is located in the northeast part of the Bohemian Massif, the easternmost segment of the European Variscides, and is composed of a few tectonically dismembered mafic-ultramafic massifs [36,37]. Previous studies on single-stage aqueous mineral carbonation of ultramafic rocks from the CSO have demonstrated that serpentinized peridotite from the BBM exhibits the highest reactivity and susceptibility to carbon mineralization [38]. Accordingly, this rock was selected for experimental studies to investigate the fate of Ni during single-stage carbonation. A serpentinized peridotite sample was obtained during fieldwork from the wall of an open-pit magnesite mine situated in the western part of the BBM (50º32'33.791"N, 16º45'47.123"E).

2.2. Whole-rock chemical analysis

The whole-rock chemistry of serpentinized peridotite before and after the carbonation experiment was analyzed in the laboratories of Bureau Veritas Commodities in Canada. This analysis involved a lithium borate fusion and a quantitative examination of major oxides and trace elements using inductively coupled plasma mass and atomic emission spectrometry (ICP-MS and ICP-ES). For this procedure, the analytical reproducibility (2σ), as estimated from five measurements of standards STD SO-19 (reference material for whole rock analysis) ranges from 0.07 % (MgO and CaO) to 0.45 % (SiO_2) at 95 % confidence limits. Analytical accuracy (2σ) based on the measurements of standards ranges from 0.03 % (MgO and CaO) to 0.2 % (SiO_2) at 95 % confidence limits. Total carbon (TOT/C) content in samples was determined using the Leco method. Loss on ignition (LOI) was measured by the weight difference after a 4-hour ignition at 1000 °C. Whole-rock chemical analyses of the serpentinized peridotite before carbonation were conducted on two types of material: one bulk sample, consisting of solid, uncrushed rock, and one powdered and sieved equivalent (particle size <50 μm). The analysis of both bulk and powder samples aimed to determine whether mineral sorting occurs during mechanical sieving and whether the powder intended for the carbonation experiment corresponds to the chemical composition of the bulk sample.

2.3. Petrographic and chemical in situ characterization

2.3.1. Starting material

The mineral composition of serpentinized peridotite was studied using a Zeiss Axioscope petrographic microscope under transmitted and reflected light conditions. A preliminary analysis of serpentinized peridotite, prepared as a carbon-coated thin section, was conducted using a JEOL JSM-IT100 scanning electron microscope (SEM) at the University of Wrocław, combined with an Oxford Instruments X-act energy-dispersive X-ray spectrometer (EDS). Measurements were performed in a high vacuum at an accelerating voltage of 15–20 kV, with a counting time of 40 seconds per analytical spot. The chemical composition of rock-forming and accessory minerals in serpentinized peridotite was conducted by electron microprobe (EMPA) Cameca SX-100 at the Faculty of Geology, University of Warsaw. Point measurements were acquired with an acceleration voltage set at 15 kV and a beam current of 25 nA. The counting time duration varied depending on the analyzed mineral to achieve the lowest possible detection limits for nickel, chromium, and cobalt. Studied thin sections were coated with a 10 nm thick carbon layer for conductivity. To ensure high-quality analyses, the following set of standards was used; standard (element): albite (Na), diopside (Mg, Si, Ca), Fe_2O_3 (Fe), rhodonite (Mn), rutile (Ti), NiO (Ni), CoO (Co), Cr_2O_3 (Cr), $LaPO_4$ (P).

2.3.2. Post-carbonation material

The imaging and chemical analysis of the post-carbonation products were conducted using a Quanta 3D FEG Dual Beam emission scanning electron microscope (FESEM) equipped with an EDAX energy dispersive spectroscopy (EDS) system at the German Research Centre for Geosciences (GFZ) in Potsdam. Field emission scanning electron microscope operated with energy-dispersive X-ray analysis at an accelerating voltage of 20 keV and 45 nA beam current. To remove the fine particles and improve SEM imaging quality, the post-experimental powder was placed into a polypropylene vial and filled with isopropyl alcohol. Subsequently, the vial underwent ultrasonic cleaning for several minutes. In the following step, dried post-experiment material was mounted onto aluminium stubs and coated with a 10 nm thick carbon layer for conductivity. Additionally, a high-resolution secondary electron (in-lens) imaging of magnesite crystals morphology was performed at the British Geological Survey, using Zeiss Sigma 300 VP-FEG FESEM at 5 kV. The material was analyzed as carbon sputter-coated (approximately 25 nm thick) powder mounted onto an aluminium stub.

2.4. X-ray powder diffraction

Prior to analysis, the starting and post-carbonation materials were mixed with ethanol and ground using corundum grinding elements in a Retsch McCrone mill. The samples were then dried at room temperature for 24 hours and homogenized using an agate mortar and pestle. The obtained powders were encapsulated in capillaries (Hilgenberg, special glass no. 10) with a diameter of 0.5 mm and wall thickness of 0.01 mm by a vertical manual charging process.

The XRD analysis was conducted with a Panalytical X'Pert Pro MPD powder diffractometer (Faculty of Geology at the University of Warsaw) equipped with a capillary spinner stage. The diffractometer was operated at 40 kV and 40 mA with a line-focus X-ray tube generating CoKα radiation ($\lambda K\alpha 1 = 1.7890100$ Å). The XRD patterns were recorded at room temperature in coupled 2θ/θ transmission mode with a step size of 0.013 °2θ and a counting time of 5 s per step over a range of 5.007–77.998 °2θ. The instrument configuration included a 240 mm radius incident beam, parabolic mirror, 0.04 rad Soller slit, and a 1 mm fixed divergence slit. The diffracted beam setup featured a 240 mm radius, 7.5 mm anti-scatter slit, 0.04 rad Soller slit, and a PIXcel detector with an active length of 3.347°. Phase identification was performed by comparing the recorded diffractograms with the patterns from the ICDD PDF-5 + database using Bruker Diffrac.Eva software (ver. 5.0.0.22). Quantitative phase analysis via Rietveld Refinement was performed using the XRD patterns of the starting and post-experimental materials with Diffrac.Topas (version 6.0). The reliability of the Rietveld Refinement is indicated by the parameter Rwp = 8.81 for the starting material and Rwp = 7.79 for the post-experimental material, demonstrating the constructed refinement model to be reliable.

2.5. Experimental procedure

Serpentinized peridotite was ground in an agate jar using a planetary ball mill (Retsch PM 100) for 40 minutes at a milling speed of 500 rotations per minute under dry and ambient temperature conditions. Ground serpentinized peridotite was sieved through a 50 μm aperture sieve to obtain a fine powder with a smaller particle size for faster reaction kinetics. The carbonation experiment was conducted using a batch-type high-pressure and high-temperature autoclave (Novoclave by Büchi AG, Switzerland). The experiment involved placing 15 g of pulverized and sieved starting material into a 200 mL Hastelloy® reaction vessel. To achieve a fluid-rock ratio of 10:1, 150 mL of ultrapure water (ISO 3696) was added to the reactor. To prevent undesirable fluid and CO_2 leakage, the vessel was sealed with Viton® O-ring seals. In the following step, the reactor was pressurized with CO_2 (>99.995 % purity) to approximately 50 bar. After several minutes, the reactor was heated to an operating temperature of 185 °C and pressurized to the desired 100 bar. The mineral composition of the serpentinized peridotite selected for the carbonation experiment is dominated by olivine Mg end-member, forsterite (Mg_2SiO_4). It was proven that the temperature of 185°C aligns with the optimal conditions for the most efficient forsterite carbonation over a range of partial pressure of CO_2 (P_{CO_2}) [19,39–42]. A mechanical stirrer was not used in this experiment. A diagram illustrating the carbonation system is shown in Fig. 1. After 96 h, the reactor was slowly cooled to 35–40°C and gradually depressurized. Fluid was sampled directly from the reaction vessel shortly after the completion of the experiment and subsequently filtered through a 0.2 μm nylon syringe filter. For further cations analysis, a portion of the fluid was acidified with nitric acid (HNO_3) (50 %) to prevent secondary precipitation. After complete fluid extraction from the vessel, post-carbonation solids were sampled. Due to the strong solidification, a chisel and hammer were used to remove the solid from the vessel. The solids were then dried in an oven at 24°C for the next four days.

2.6. Chemical analysis of post-carbonation fluid

Cation concentrations (Ca, Mg, Na, K, Fe, Al, Si, Mn, Cr, Ni, Co, Cu, Zn, and Sr) were determined using an Inductively Coupled Plasma – Optical Emission Spectrometer (Avio 200 ICP-OES™, PerkinElmer, Waltham, Massachusetts, USA). Conditions of analysis are reported in Supplementary Materials in Table S1. Calibration curves were constructed using a multi-element standard solution prepared from single reference ICP standard solutions (Supelco®-Merck and CPAchem). Quality control was achieved using analysis of diluted ICP-Multi Element Standard Solution IV (Supelco®-Merck). Chemical analysis of the post-carbonation fluid was performed in triplicate.

2.7. Geochemical modeling

The saturation indices (SI) and the solution ionic speciation were calculated using PHREEQC version 3.7.3 [43]. The PHREEQC input file was constructed using cation concentrations measured in the post-experimental leachate (see Table 3) and a temperature of 185 °C. The pH of the post-carbonation fluid was measured at 6.55 using a calibrated pH meter (Elemetron 410) shortly after reactor decompression. For the SI and solution ionic speciation calculations, a pH of 5.449 was employed, as determined through PHREEQC simulation. This value represents the estimated in situ pH before decompression, accounting for the influence of dissolved CO_2. To incorporate CO_2 into the calculation, CO_2 fugacity (fCO_2) was determined using the Peng-Robinson equation with Thermosolver 1.0 software [44,45]. With a CO_2 fugacity coefficient of 0.8934 at 100 bar and 185 °C, the resulting fCO_2 is 89.3 bar. The input files used for speciation and saturation-index calculations are available in the supplementary materials. Activity and predominance diagrams have been constructed using Geochemist's Workbench® (GWB) software packages. The thermodynamic properties of minerals and molecules for PHREEQC and GWB calculations were sourced from the Thermoddem V1.10 thermodynamic database, provided by the Bureau de Recherches Géologiques et Minières [46].

2.8. Nickel mass balance

Ni distribution before and after the carbonation experiment was estimated using average Ni contents in forsterite, serpentine, tremolite, spinel, and sulfides measured in this study. The proportions of minerals were based on the Rietveld Refinement analyses. The Ni concentration in clinochlore was taken from the study of Kierczak et al. [47]. The proportion of sulfides was calculated from the total sulfur concentration (TOT/S) in the whole rock. Ni concentration in Ni-phyllosilicate was sourced from EDS analyses. For estimating the experiment budget, we

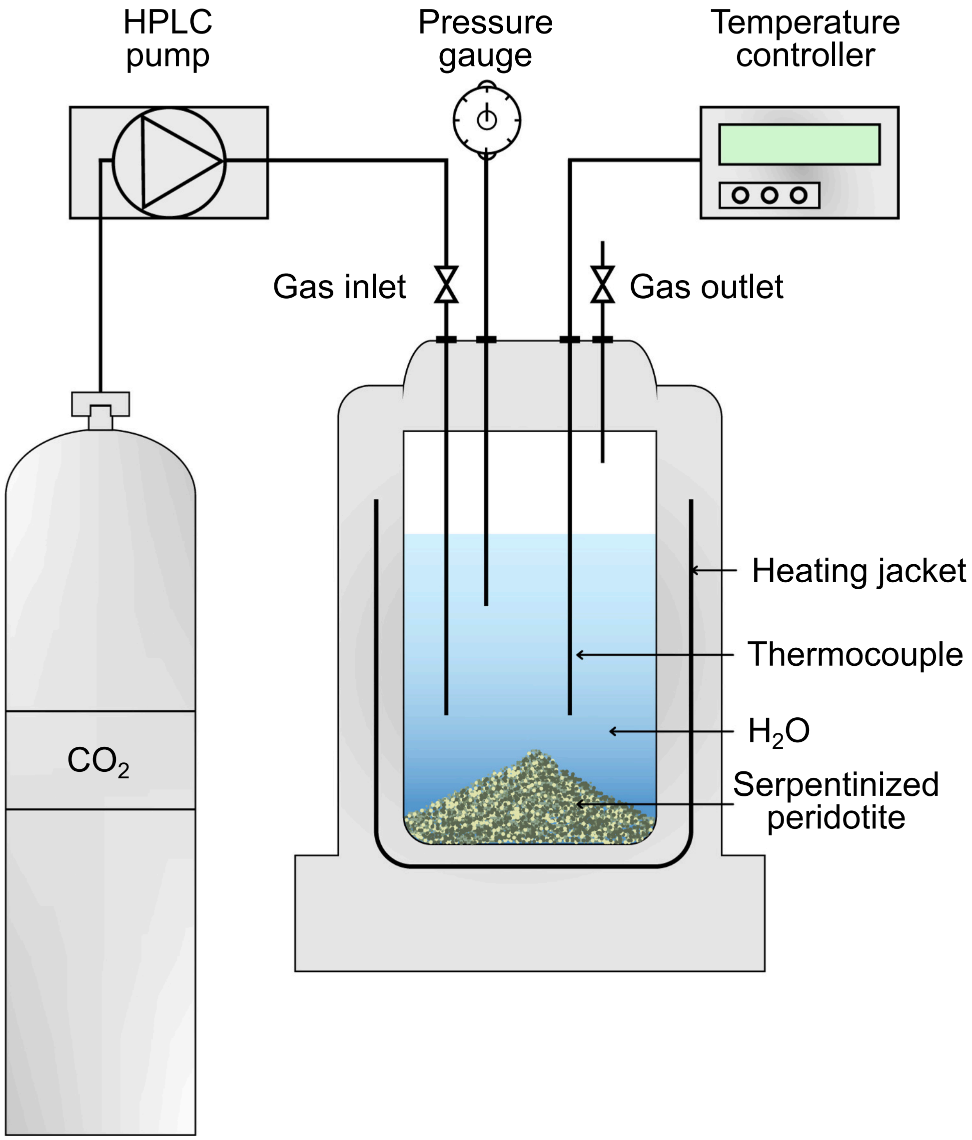

Fig. 1. Scheme of the setup used for the single-stage aqueous mineral carbonation experiment.

used Ni content in natural magnesite from the studied area [48]. To assess the potential incorporation of Ni into secondary Ni-phyllosilicates, the total Ni content was fixed at the value measured in the post-experimental solid by whole-rock analysis, while the proportion of Ni-phyllosilicate was treated as an unknown variable.

3. Results

3.1. Whole-rock chemical composition

The serpentinized peridotite bulk and powdered samples demonstrated comparable compositions concerning major oxide content, LOI, and TOT/C. Serpentinized peridotite from BBM showed typical Ni concentrations for the Earth's upper mantle, averaging 2000 mg/kg [49].

After the carbonation experiment, the material contained slightly different concentrations than the starting material (powder). There was a clear decrease in the content of silica (SiO_2) (decrease by 7.37 wt%) and Mg oxide (MgO) (decrease by 7.81 wt%). The concentrations of the remaining major oxides were slightly lower than those of the starting material. However, these decreases were balanced by a substantial increase in the LOI value, which rose by 17.4 %, and in the TOT/C, which increased by 5.28 %. The Ni content in post-carbonation material reached 2304 mg/kg, while Cr and Co contents showed a reduction. Table 1 provides a comparative overview of the whole-rock chemical compositions of bulk and powdered serpentinized peridotite samples from BBM alongside the post-carbonation materials. Supplementary materials (Table S2) provide a comparison of other trace elements analyzed before and after carbonation.

3.2. X-ray powder diffraction

Quantitative and qualitative analyses using X-ray powder diffraction were performed to identify the solid products of the mineral carbonation experiment and evaluate compositional changes relative to the starting material. The diffractograms obtained demonstrated significant changes in the phase composition of the serpentinized peridotite during the carbonation (Fig. 2). All of the phases present in the unreacted material were less abundant after the experiment, with the largest decrease observed for forsterite proportion. Rietveld Refinement suggested that 42 % of forsterite was dissolved during the experiment (Table 2). Instead, approximately 46 % magnesite was formed in the post-carbonation material.

Table 1
The serpentinized peridotite whole-rock chemical composition for bulk and powdered samples before and after mineral carbonation. Nickel, chromium, and cobalt are included in the total (wt%) in their oxide forms.

Serpentinized peridotite			
	Bulk sample	Powdered sample	After carbonation (using powdered sample)
SiO_2 *(wt%)*	41.07	40.48	33.11
MgO *(wt%)*	37.46	37.98	30.17
Fe_2O_3 *(wt%)*	8.95	8.86	7.22
CaO *(wt%)*	1.84	1.24	0.97
Al_2O_3 *(wt%)*	0.33	0.47	0.38
LOI *(wt%)*	9.0	9.5	26.9
Ni *(mg/kg)*	1911	2034	2304
Cr *(mg/kg)*	2065	2341	1984
Co *(mg/kg)*	118	122	88.7
Total *(wt%)*	99.28	99.33	99.05
TOT/S *(%)*	0.02	0.03	0.04
TOT/C *(%)*	0.47	0.46	5.74

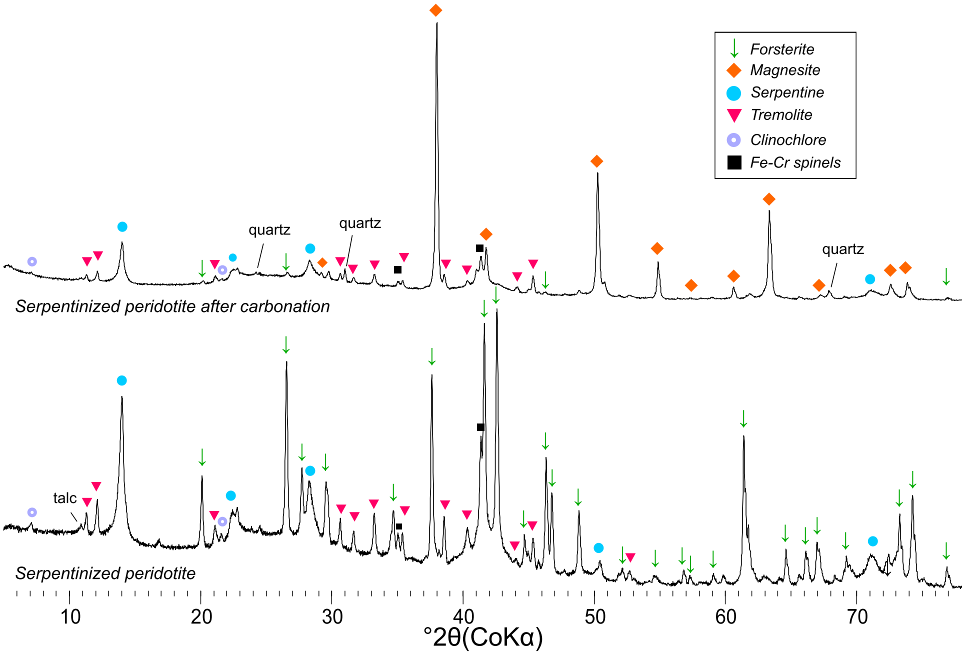

Fig. 2. Comparison of XRD patterns of unreacted (pre-experiment) and carbonated (post-experiment) serpentinized peridotites from the Braszowice-Brzeźnica Massif. Note the lack of forsterite and the dominance of magnesite in the carbonated sample.

Table 2
Comparison of the phases present in the unreacted serpentinized peridotite from BBM and the same sample after the single-stage aqueous carbonation experiment. Quantitative data (wt%) were acquired through Rietveld Refinement.

	Serpentinized peridotite	
Mineral name	before carbonation (*wt%*)	After carbonation (*wt%*)
Forsterite	48.0	6.0
Serpentine	13.6	9.7
Tremolite	10.3	5.63
Clinochlore	16.7	12.9
Fe-Cr spinels	0.55	0.49
Magnesite	0.00	46.0

3.3. *Petrography and mineral chemistry*

3.3.1. *Starting material*

The mineral composition of serpentinized peridotite was primarily comprised of forsterite ($Fo_{89–90}$). The rock also contained a significant presence of serpentine minerals and tremolite. The most common accessory minerals present in the rock were Fe-Cr spinels. Serpentinized peridotites in BBM were characterized by a ribbon-shaped mesh texture, where microscopic serpentine veins cross-cut forsterite grains (Fig. 3a). Tremolite occurred as blady and elongated crystals, often cut by serpentine veinlets (Fig. 3b). Smaller magnetite grains (up to a few µm) were typically associated with serpentinite-dominated zones (Fig. 3c). The largest individual crystals of Fe-Cr spinels reached 1 mm and exhibited a well-preserved chromiferous core surrounded by magnetite or chromian magnetite. Clinochlore aggregates partially replaced many primary spinels, appearing as inclusions or aureoles. Additionally, there were very rare diopside relicts, dolomite grains within serpentine veins (Fig. 3d), and < 8µm Ni-Fe sulfides grains, including millerite and pentlandite (Fig. 3e). A summary of the chemical composition of individual mineral phases, obtained through EMPA spot analysis, was provided in the supplementary materials (Table S3).

EMPA analyses ($n = 50$) revealed that Ni concentrations in forsterite did not exceed 0.34 wt%, which was consistent with mantle-derived forsterite, typically containing an average of approximately 0.3 wt% Ni [50,51]. The second most abundant phase in the studied peridotites was the serpentine subgroup minerals, however, their Ni concentrations ($n = 8$) did not exceed 0.29 wt%. Tremolite showed the lowest Ni content ($n = 7$), with concentrations below 0.1 wt%. Among Fe-Cr spinels

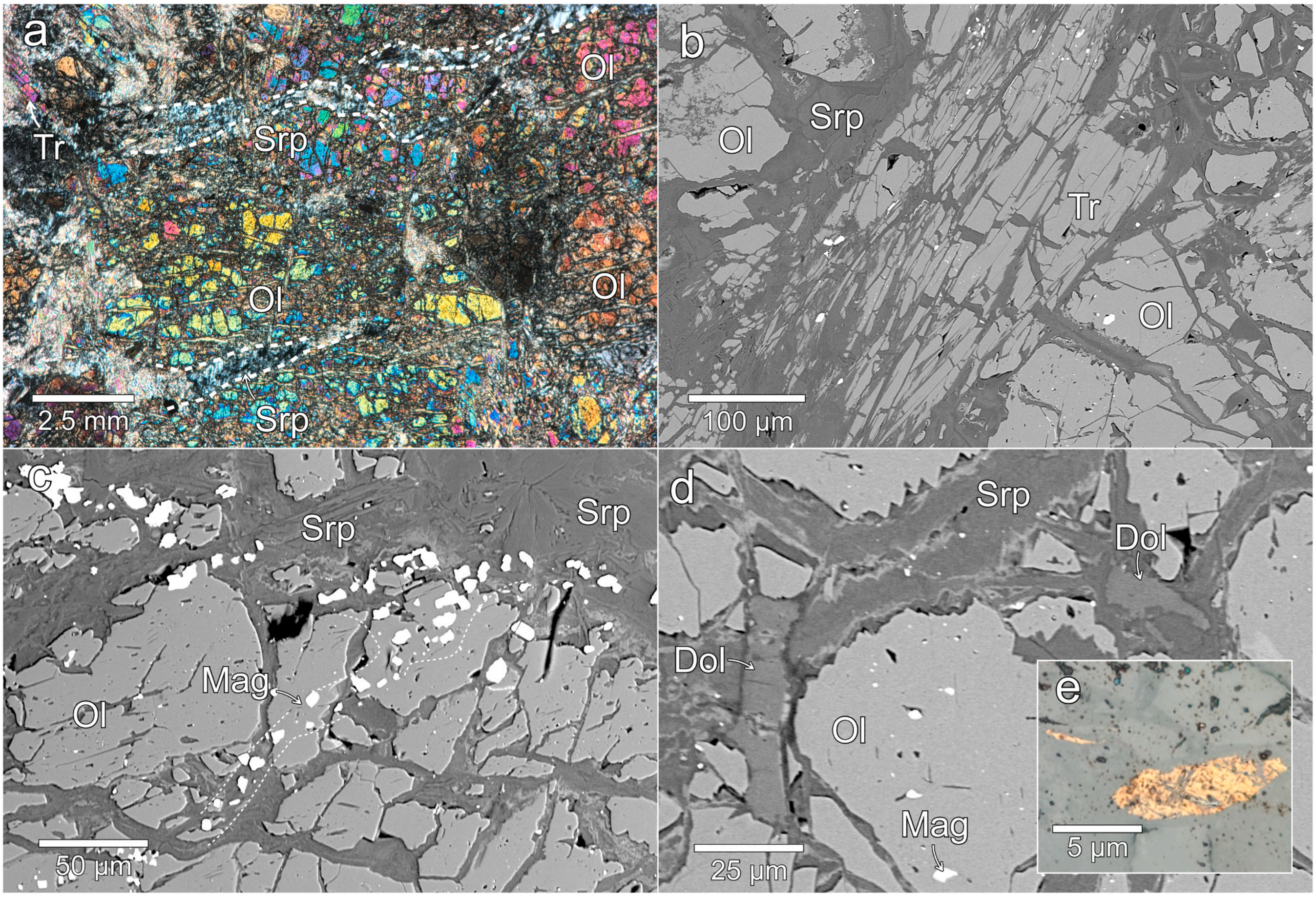

Fig. 3. Microscopic (a, e) and back-scattered electron (b,c,d) images of serpentinized peridotite from Braszowice-Brzeźnica massif before mechanical activation (thin section). (Ol – olivine, Srp – minerals from the serpentine subgroup, Mag- magnetite, Tr- tremolite, Dol- dolomite). The rock predominantly comprises anhedral olivine grains (a), and bladed tremolite crystals (b) cross-cut by serpentine veinlets. Magnetite and chromium magnetite occur mostly as scattered, irregular grains (c). Rare dolomite is present, mostly within serpentines (d). A reflected light image of pentlandite is presented in figure (e).

(n = 14), two distinct groups were observed (Fig. 4). The first group, with lower Ni content, corresponded to chromiferous cores, where Ni concentrations remained below 0.1 wt%. These cores also showed elevated Mg and Al concentrations (see Table S3). In contrast, higher Ni concentrations were observed in magnetite rims and grains, typically remaining below 0.5 wt%. Sulfides, although scarce, contained the highest Ni concentrations, with millerite (n = 10) showing 58.1–68.4 wt % Ni and pentlandite (n = 9) 30.7–33.6 wt% Ni.

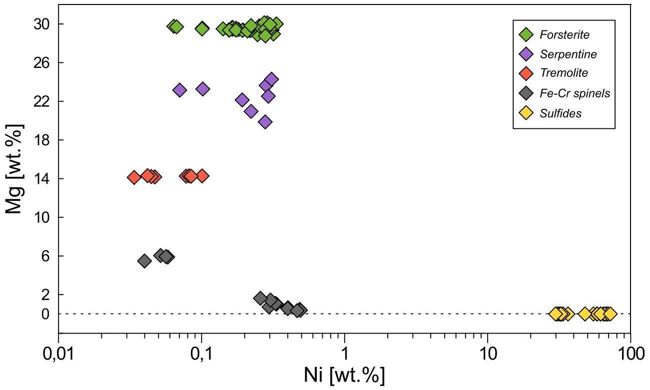

Fig. 4. Scatter plot of Mg (wt%) vs. Ni (wt%) showing EMPA analysis for forsterite, serpentine, tremolite, Fe-Cr spinels, and sulfides, illustrating the distribution of Ni across individual mineral phases in serpentinized peridotites from BBM. For sulfides, Mg concentrations were set to the value of "0" due to the absence of Mg analyses. Note that values on the x-axis are displayed on a logarithmic scale.

3.3.2. Post-carbonation material

FESEM analyses revealed the details of magnesite crystals formed during the carbonation experiment. Magnesite appeared as < 8 µm euhedral, rhomboid-shaped crystals (Fig. 5a), locally cementing unreacted powder of serpentinized peridotite. Magnesite was observed to have undergone partial recrystallization, resulting in the formation of a cryptocrystalline matrix that frequently acted as a cementing agent for the undissolved fine rock particles (Fig. 5b). All analyzed magnesites exhibited a typical chemical composition of approximately 48.0 wt% MgO and 52.0 wt% CO_2.

The XRD diffractogram of the solid products displayed peaks at characteristic positions for quartz (see Fig. 2), indicating the formation of small quantities of crystalline SiO_2 during carbonation. FESEM analyses of the post-carbonation material confirmed the presence of chalcedony layers exhibiting a distinctive botryoidal morphology (Fig. 6a). Some of the chalcedony-composed surfaces were additionally overgrown with another layer of Ni phyllosilicates (Fig. 6b). The direct contact between chalcedony and the layer of Ni phyllosilicate was most visible at the edge of the observed structures or in the central parts of the nodules (Fig. 6c, Fig. 6d). A homogeneous rectangular area (5 µm × 8 µm), within the Ni phyllosilicate layer, was analyzed for its chemical composition, revealing 41 wt% SiO_2, 35 wt% NiO, and 6 wt% MgO. Honeycomb-like and cornflake textures [52], visible in BSE images, suggested that the Ni silicates might belong to the smectite group.

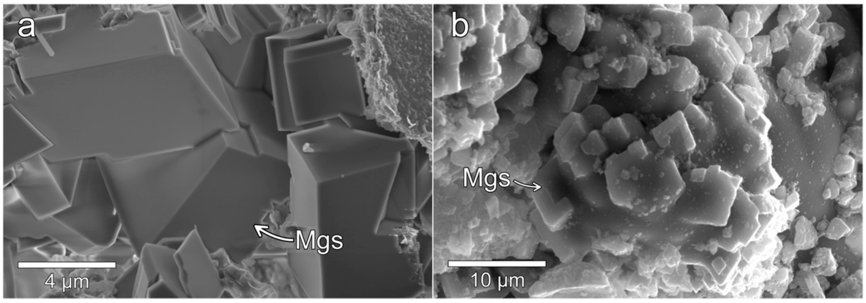

Fig. 5. Back-scattered electron (BSE) images of (a) single euhedral magnesite (Mgs) crystal surrounded by ultramafic, unreacted fines and; (b) magnesite (Mgs) recrystallized aggregates.

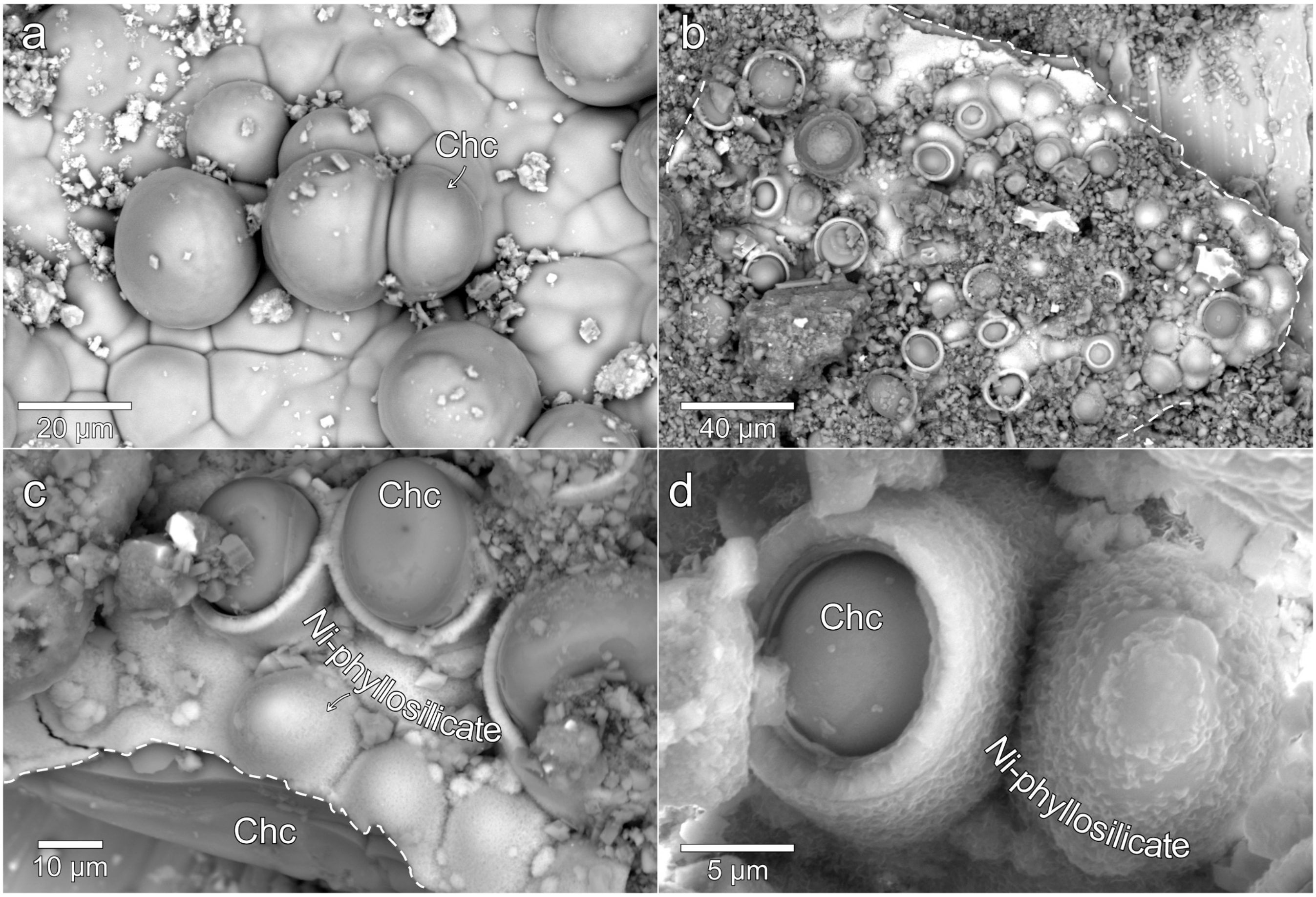

Fig. 6. Back-scattered electron (BSE) images of (a) naked chalcedony (Chc) layer with characteristic nodules on its surface; (b) chalcedony layer overgrown with Ni-phyllosilicate layer (c) the contact between the chalcedony layer and Ni silicates; (d) a close-up image of two silica nodules, where Ni-phyllosilicate completely overgrows one nodule while the second remains exposed.

3.4. *Chemical composition of post-carbonation fluid*

The triplicate analysis of cation concentrations in the post-experimental leachate revealed that Si and Mg exhibited the highest average concentrations, reaching 3360 mg/kg and 679 mg/kg, respectively. The element with the third highest concentration was Ni, with an

Table 3
The triplicate analysis (I – III) of the chemical composition of the post-experimental leachate. The average concentrations, listed in the last row, were used for geochemical modeling.

mg/kg	Ca	Mg	Na	K	Fe	Al	Si	Mn	Cr	Ni	Co	Sr
I	13.1	687	10.9	2.31	4.41	0.021	3360	1.20	0.05	17.5	0.04	0.30
II	12.6	667	10.4	2.46	4.35	0.021	3337	1.18	0.05	17.5	0.04	0.29
III	13.0	684	11.0	2.33	4.59	0.021	3382	1.21	0.05	17.7	0.05	0.30
avg.	12.9	679	10.8	2.37	4.45	0.021	3360	1.20	0.05	17.6	0.04	0.30

average concentration of 17.6 mg/kg. The Ca and Fe content in the post-experimental leachate was 12.9 mg/kg and 4.45 mg/kg, respectively. The complete chemical composition of the fluid is summarized in Table 3.

3.5. Nickel mass balance model

In the proposed model, the Ni budget in serpentinized peridotite, before mineral carbonation, was estimated based on the quantitative distribution of individual mineral phases and their respective Ni concentrations (Table 4). Despite some uncertainties, such as (1) the average Ni concentration in sulfides that included both pentlandite and millerite, and (2) the average concentration of Ni in spinels that included Cr-rich and Fe-rich types, the Ni budget calculated before the experiment (total) approximated the Ni concentration in the whole rock (*WR*).

The same methodological approach was applied to determine Ni distribution in the post-experimental material. Based on this analysis, the proportion of Ni-phyllosilicate required to balance the Ni budget (*WR* = 2305 mg/kg of Ni) was estimated to be no more than 1 wt%, and was likely closer to 0.5 wt% in the post-carbonation material. Moreover, secondary magnesite, with an average Ni content of approximately 5 mg/kg, had no significant impact on controlling the overall Ni budget.

4. Discussion

Mineral carbonation occurs when gaseous CO_2 dissolves in water, forming aqueous CO_2, which undergoes hydration to produce carbonic acid (H_2CO_3). Carbonic acid then dissociates predominantly into hydrogen ions (H^+) and bicarbonate ions (HCO_3^-), with further dissociation into carbonate ions (CO_3^{2-}) depending on pH. In the presence of divalent cations, these ions can precipitate as carbonate minerals [13]. This process was documented throughout our batch experiment, during which serpentinized peridotites underwent carbonation. This discussion primarily addresses the mobility of Ni during mineral carbonation of serpentinized peridotites at 185 °C and a P_{CO_2} of 100 bar. We show that at least 50 % of Ni was mobilized and subsequently 95 % was incorporated into secondary Ni-phyllosilicate, but also several percent remained in the carbonation fluid.

4.1. Forsterite dissolution

The ultramafic feedstock used in the single-stage aqueous carbonation experiment primarily comprises forsterite, which constitutes 48.0 wt% of the whole rock and contains approximately 0.3 wt% Ni. Therefore, the extent of forsterite preservation during the carbonation of serpentinized peridotites is an essential factor controlling Ni supply to the system. A comparative analysis of XRD diffraction patterns (before and after carbonation) revealed the nearly complete absence of forsterite in the post-experimental solid. The forsterite content of approximately 6.0 wt% in the post-experimental material, as determined through Rietveld Refinement, falls within the analytical margin of error. Moreover, the presence of forsterite was not detected when observing the material using electron microscopy. This indicates that under the applied pressure, temperature, and duration, forsterite was either completely dissolved or, if any grains remained, they were so scarce that they were effectively undetectable. The complete dissolution of forsterite could be enhanced by slightly acidic pH, a condition that promotes efficient olivine dissolution [53–55]. It remains unclear whether all the forsterite fully dissolved or partially transformed into serpentine minerals. However, the decrease in both serpentine and amphibole proportions after the experiment (Table 2) suggests that other primary phases were also dissolving. Nonetheless, we propose that the extensive dissolution of forsterite was the main source of divalent cations (Mg^{2+} and Ni^{2+}) and could contribute approximately 1000 mg/kg to the mobilized Ni budget (based on the average Ni content in olivine as measured by EMPA and its initial proportion from the Rietveld Refinement). As the post-experimental fluid contained only 680 mg/kg of Mg and 18 mg/kg of Ni, the majority of these elements were probably incorporated into newly precipitated phases such as magnesite (Mg^{2+}) and Ni-phyllosilicates (Ni^{2+}).

4.2. Magnesite precipitation

Depending on the specific conditions of the mineral carbonation process, both hydrated and non-hydrated magnesium carbonate minerals can be formed [56]. Although magnesite and, for example, nesquehonite share the same Mg: C ratio (1: 1), magnesite is anhydrous, and its lower molecular weight, together with its higher CO_2 mass fraction (52 wt %), confers a much greater CO_2-storage density and long-term chemical stability, making it an attractive mineral sink for carbon storage [57]. In this study, magnesite is the only carbonate identified (SI = 1.33).

The analysis revealed no detectable Ni content in the studied magnesite crystals. Furthermore, XRD analysis did not identify the presence of the gaspéite, a Ni end-member of the $(Mg,Ni)CO_3$ solid solution series, among the solid products of our carbonation experiment. In nature, gaspéite is a very rare mineral [58], but it was synthesized in laboratory conditions at 250 °C, pH approximately 4, and approximately

Table 4

Nickel balance model before and after single-stage aqueous mineral carbonation.

Before mineral carbonation			
	Mineral proportions [*wt%*]	Ni content [*mg/kg*]	Contribution to total Ni budget [*mg/kg*]
Forsterite	48.00	2260	1084.8
Serpentines	14.00	1500	204
Tremolite	10.00	680	70.04
Clinochlore	17.00	1886	314
Fe-Cr spinel	0.55	2500	13.75
Sulfides	0.09	450000	405
Total			2092
WR [mg/kg]			2034
After mineral carbonation			
	Mineral proportions [*wt%]*	Ni content [*mg/kg*]	Contribution to total Ni budget [*mg/kg]*
Forsterite	6.00	2260	135.6
Serpentines	9.70	1500	145.5
Tremolite	6.00	680	40.8
Clinochlore	12.9	1886	243.3
Fe-Cr spinel	0.49	2500	125
Sulfides	0.09	450000	405
Magnesite	46.00	5	2.3
Ni-phyllosilicate	0.50	261100	1306
WR [mg/kg]			2304

40 atm of P_{CO_2} [59]. The calculated SI for $NiCO_3$ is 2.03, indicating the potential for its precipitation. We suggest that gaspéite did not form in this study because carbonate ions preferentially form chemical bonds with Mg^{2+} rather than Ni^{2+} [60], particularly when Mg^{2+} is significantly more abundant in the solution.

4.3. Silica precipitation

Various forms of silica are a common by-product of mineral carbonation, using forsterite-bearing rocks [20,61–63]. The presence of silica in the system is consistent with the course of the carbonation reaction [64]. As Mg, rather than Si, combines with carbonate ions during the dissolution of forsterite, silicon concentration in the solution continuously increases. This process typically continues until the system reaches amorphous silica saturation (the point where precipitation may start). Studies have shown that silicon in the post-carbonation fluid primarily exists in the form of orthosilicic acid (H_4SiO_4) [65,66], a result also confirmed in our experiment by fluid speciation modeling.

Qualitative and quantitative XRD analysis revealed a small amount of quartz in the post-experimental solid, estimated at 1.7 wt%. During SEM-BSE studies, prismatic quartz crystals were not observed among the solid products. However, chalcedony and quartz exhibit overlapping XRD peaks, particularly around the 2θ position at 26.6°, due to the presence of 50–100 nm α-quartz crystallites as components of chalcedony [67]. Therefore, the XRD patterns align more closely with chalcedony, as confirmed by BSE imaging observations. Chalcedony occurs as a layered structure with numerous nodules on its surface. This distinctive morphology, characterized by a hemispherical texture, is called botryoidal and is a commonly observed feature of chalcedony [68]. The calculated SI of 1.36 suggests that the solution was supersaturated with respect to chalcedony, indicating a tendency for it to precipitate from the solution during the carbonation experiment. It is also noteworthy that the chalcedony precipitated as a flat and relatively extensive layer (approximately 250 μm in length), which may suggest that it crystallized on the inner wall of the vessel and subsequently fell into the reacted ultramafic fines during or shortly after reactor decompression.

The precipitation of a chalcedony layer may be essential for promoting smectite growth, which can serve as a sink for transition metals and play a key role in controlling Ni mobilization. Experimental studies at similar temperatures (100–150 °C) have shown that quartz supplies additional silica to the solution, which is crucial for smectite crystallization on the surface of quartz [69]. Chalcedony formation during single-stage carbonation may provoke the growth of smectite minerals by increasing silica activity in the solution, thereby promoting smectite nucleation and growth on the clean chalcedony layer.

4.4. Formation of Ni-phyllosilicates

The presence of Ni-phyllosilicates among post-carbonation solid products strongly correlates with chalcedony. It was observed that the chalcedony layer is extensively overlaid by a thin (< 5 μm) mineral layer. This coating is predominantly compositionally homogenous, although there are areas where the underlying silica layer remains exposed (see Fig. 6b).

Electron microscopy analysis revealed a distinct honeycomb structure, a characteristic feature of the smectite group [52]. Analogous textures were observed in nature during the growth of smectite layers on sand grains, where detrital quartz probably plays an important role as a source of silica necessary for smectite formation [70].

On a laboratory scale, Ni phyllosilicates, visually resembling those formed during our carbonation experiment, have been synthesized as precursors for Ni/SiO_2 catalysts [71]. Similar Ni phyllosilicates, in the form of spherical particles, have been synthesized as reusable catalysts and versatile catalytic support materials for the chemical industry [72]. Also, a group of 2:1 type Ni-phyllosilicates was synthesized to develop Ni/SiO_2 catalysts for CO_2 methanation [73]. The experiments mentioned above focused on catalyst synthesis and were conducted under hydrothermal conditions with aqueous solutions, similar to the approach used in this study. Although this question remains unanswered, there is a possibility that during single-stage carbonation of ultramafic rocks with high Ni content, byproducts resembling Ni/SiO_2 catalysts could be synthesized.

To the best of our knowledge, there are no direct reports in the literature of Ni-phyllosilicate crystallization as a by-product during the experimental mineral carbonation of ultramafic rocks. In natural settings, different Ni-phyllosilicates are frequently observed as products of the lateritization of ultramafic rocks [74,75]. Water plays a crucial role in this process by facilitating the dissolution of silicates and the subsequent release of Mg^{2+} and Ni^{2+} cations, which are then incorporated into newly formed phyllosilicates. Additionally, when sufficiently enriched with CO_2, water can promote the precipitation of carbonates, contributing to the formation of magnesite within weathered ultramafic massifs [76]. The P-T (185 °C and P_{CO_2} of 100 bar) conditions inside the experimental reactor used in this study, although much higher than those typical of tropical weathering, resemble accelerated lateritization.

The conditions inside the reactor significantly exceeded those typical of tropical weathering, a comparatively low-temperature process when contrasted with hydrothermal or magmatic activity. Despite these temperature discrepancies, the process may still resemble lateritization and, therefore, the formation of secondary Ni ores, with the applied 185 °C and P_{CO_2} of 100 bar, significantly enhancing and accelerating this process.

Nickel speciation and activity plot of log $(aMg^{2+})/(aH^{+})^2$ vs. log $aSiO_2$ are used to identify the potential Ni-bearing phyllosilicates at equilibrium with the fluid in the 96th hour of carbonation experiments (shortly before reactor decompression). The speciation diagram for the Ni in the CO_2-H_2O system indicates that Ni^{2+} is the dominant species in solution (Fig. 7a). The activity plot was constructed for the MgO-SiO_2-Al_2O_3-H_2O system at 185 °C and solution pH of 5.44, corresponding to the final stage of the experiment. The applied system could not be extended to NiO due to the unavailability of the equilibrium coefficient (log K) for Ni-end-member phyllosilicates at temperatures above 25°C [77]. The activity plot (Fig. 7b) shows that after 96 hours, equilibrium was reached for Mg-saponite [$Mg_{0.17}Mg_3Al_{0.34}Si_{3.66}O_{10}(OH)_2$] (acc. Thermoddem database). Saponite and its varieties are 2:1 trioctahedral phyllosilicates and belong to the smectite group [78]. The precipitation of Mg-saponite is also supported by a high SI of (>12) after 96 hours of the experiment. However, the measured chemical composition of the precipitates does not correspond to the Mg-rich saponite, primarily due to the absence of aluminium and the exceptionally high NiO content (approximately 35.00 wt%). Since Ni^{2+} was nickel dominant ion species at the experiment final stage, it could replace Mg^{2+}, especially as most of the Mg was consumed by carbonate ions. Wang and Dreisinger [79] described the “complex competition of divalent metals” during the mineral carbonation of olivine, where Ni^{2+} and Mg^{2+} compete to form stable complexes, with Mg^{2+} predominantly combining with carbonate ions to precipitate as Mg carbonates. We hypothesize that the Ni content in the fluid would either increase over time or combine with other ions to form more complex compounds, such as phyllosilicates, rather than carbonates. The nickeliferous smectites found among post-carbonation solids in our experiment may represent a Ni-rich, Al-free variant of saponite-like phases. Nonetheless, without detailed crystallographic data for this Ni-rich phase, assigning a definitive nomenclature remains challenging, warranting further investigation. Due to many challenges (intimate mixtures, fine-grained nature) in characterizing and classifying these minerals, researchers commonly use the term “garnierites” to describe Ni-Mg phyllosilicates occurring in lateritic covers of ultramafic rocks [80]. Similarly, the Ni-rich phase that crystallized in our experiment may be classified under the term “garnierite”. Given the data obtained and the specific formation conditions, this designation appears to be more scientifically accurate.

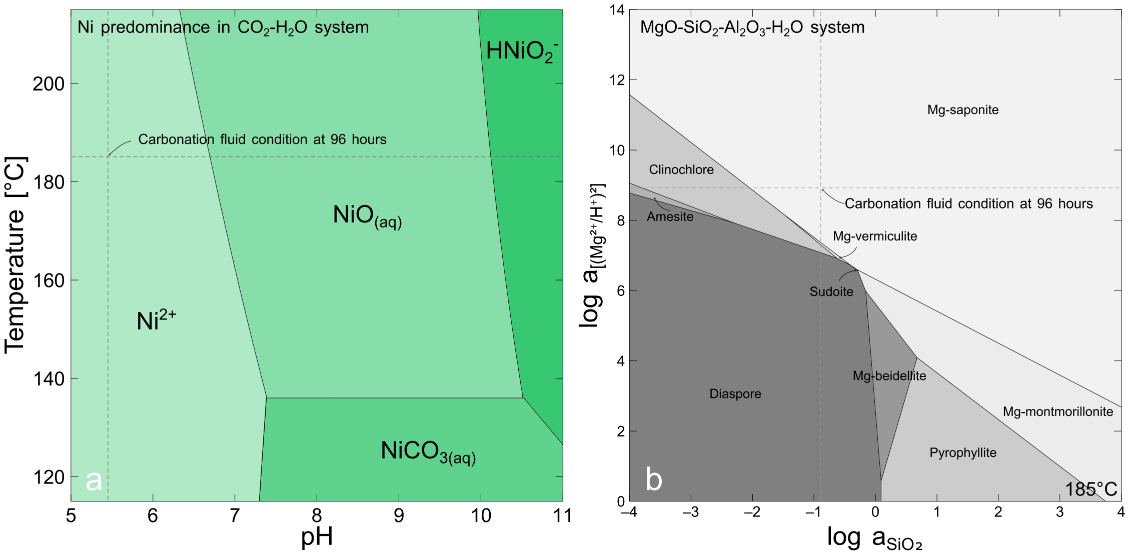

Fig. 7. (a) Nickel predominance (T vs. pH) diagram in CO_2-H_2O system at 185 °C; (b. Activity plot of log a[$(Mg^{2+}/H^+)^2$] vs. log $aSiO_2$ for the system MgO-SiO_2-Al_2O_3-H_2O at 185 °C and pH 5.44. The thermodynamic properties of minerals and molecules were sourced from the Thermoddem V1.10 thermodynamic database.

4.5. Nickel mobilization to fluid

Chemical analysis of the post-experimental fluid revealed that under the applied temperature and P_{CO_2}, Ni was mobilized into the solution, reaching concentrations of an average of approximately 18 mg/kg. It is possible that the Ni concentration was higher during the experiment and may have continued to increase until Ni-rich phases began to precipitate. The approximately 18 mg/kg of Ni in the post-carbonation fluid was achieved after 96 h.

Although the literature on Ni mobilization during ex situ mineral carbonation and olivine dissolution are scarce, related natural science research offers valuable insights. Montserrat et al. [81] demonstrated in laboratory experiments that olivine dissolves steadily in seawater with increasing Ni concentrations, proposing that Ni can effectively serve as a proxy for tracking olivine dissolution rates. It was also noted that the release of Ni into seawater could exceed safe thresholds, potentially affecting marine life, particularly in coastal areas with limited water exchange. Groundwaters associated with ophiolitic complexes typically show Ni concentrations below 50 ppb, which are significantly lower than those observed in post-carbonation fluid [82–84]. In contrast, analysis of Ni mobility in soil using EDTA extraction shows that up to 5 % (over 100 mg/kg) of Ni can be leached from ultramafic rocks, which are higher than the Ni levels observed in post-carbonation fluids. There is currently no available literature on the formation of Ni-bearing phases following EDTA extraction, as it is believed that plants absorb most of the extracted Ni. In our study, the nickel released from olivine dissolution was primarily associated with secondary phases, which results in the lower Ni-content in the final extraction fluid compared to Ni content in fluids related to ultramafic rocks weathering [47].

4.6. Nickel distribution before and after carbonation

Ni mass balance model suggests that at least 50 % of Ni was removed from the serpentinized peridotite (approximately 1000 mg/kg). Also, the low concentration of Ni in post-experimental fluid (approximately 18 mg/kg) and high in post-experimental solid (2300 mg/kg) indicate that most mobilized Ni must have been included in secondary phases. The only Ni-bearing secondary phase identified in post-experimental products was Ni-phyllosilicate with a measured Ni concentration of approximately 26 wt%. Although Rietveld Refinement did not detect this phase, its high Ni content suggests that even a small amount, as little as 0.5 %, could account for the over 1000 mg/kg of Ni released. This likely corresponds to the whole of the Ni derived from forsterite dissolution (see Table 4). Mass-balance calculations involve some uncertainty, particularly regarding the unknown fate of sulfides, a primary Ni-bearing phase. Nevertheless, these calculations suggest that more than half of the Ni can be mobilized during carbonation, with the majority (approximately 98 %) eventually immobilized in a relatively small fraction of secondary phyllosilicate.

5. Conclusions

The single-stage aqueous mineral carbonation of serpentinized peridotite, performed at 185 °C under a partial CO_2 pressure of 100 bar for 96 hours, led to significant forsterite dissolution and magnesite precipitation. Under these carbonation conditions, forsterite dissolution regulated the Ni supply to the system. This study revealed that Ni^{2+} was primarily incorporated into newly formed phyllosilicates, while some remained in the aqueous fluid. No Ni was detected in newly crystallized magnesite. The Ni-phyllosilicates formed during single-stage carbonation had a high Ni concentration and were the main contributors to the Ni budget in the post-carbonation material despite their overall quantity being minimal.

Ultramafic rocks, such as the partially serpentinized peridotites used in this study, are promising candidates for single-stage aqueous mineral carbonation, offering a pathway for permanent CO_2 sequestration. However, the dissolution of forsterite-bearing ultramafic rocks is expected to release Ni, which may pose environmental risks. Our study provides insights into the mobility of Ni and raises important questions for further research around the optimization of mineral carbonation technologies with minimal environmental impact. We thus recommend monitoring the formation of potential Ni-rich phases during carbonation as well as the concentration of Ni in the carbonating fluids, particularly in future large-scale ex situ mineral carbonation projects using ultramafic rocks. Experimental results indicate that both CO_2 sequestration and the synthesis of Ni-rich phyllosilicates can be achieved through single-stage mineral carbonation. Further work is needed on the stability of the newly formed phases, and their long-term potential for Ni immobilization.

CRediT authorship contribution statement

Błażej Cieślik: Writing – original draft, Visualization, Resources, Methodology, Investigation, Funding acquisition, Formal analysis,

Conceptualization. **Alicja Lacinska**: Writing – review & editing, Investigation. **Anna Pietranik**: Writing – original draft, Formal analysis, Conceptualization. **Maciej Róziewicz**: Visualization, Investigation. **Artur Pędziwiatr**: Writing – review & editing, Investigation. **Krzysztof Turniak**: Writing – review & editing, Investigation. **Agata Łamacz**: Writing – review & editing. **Jakub Kierczak**: Writing – review & editing, Supervision, Project administration, Funding acquisition.

Declaration of Competing Interest

The authors declare that they have no known competing financial interests or personal relationships that could have appeared to influence the work reported in this paper.

Acknowledgements

This work was financially supported by the National Science Centre (NCN) in Poland in the frame of the OPUS 22 program under the grant agreement UMO-2021/43/B/ST10/01594. This project has received funding from the European Union's Horizon 2020 research and innovation programme under grant agreement No 101005611 for Transnational Access conducted at Helmholtz-Zentrum Potsdam Deutsches GeoForschungsZentrum (GFZ) as part of the Potsdam Imaging and Spectral Analysis (PISA) facility. We sincerely thank Dr. Gerardo Algara-Siller for his invaluable assistance with electron microscope imaging and Dr. Łukasz Kruszewski for his expert guidance on Rietveld Refinement.

Appendix A. Supporting information

Supplementary data associated with this article can be found in the online version at doi:10.1016/j.jcou.2025.103119.

Data Availability

Data will be made available on request.

References

[1] H.D. Matthews, S. Wynes, Current global efforts are insufficient to limit warming to 1.5°C, Science (1979) 376 (2022) 1404–1409, https://doi.org/10.1126/science.abo3378.

[2] National Oceanic and Atmospheric Administration (NOAA), Global greenhouse gas reference network: CO_2 trends, ⟨Https://Gml.Noaa.Gov/Ccgg/Trends/⟩ (2024). ⟨https://gml.noaa.gov/ccgg/trends/⟩ (Accessed March 13, 2025).

[3] S. Anderson, R. Newell, Prospects for carbon capture and storage technologies, Annu. Rev. Environ. Resour. 29 (2004) 109–142, https://doi.org/10.1146/annurev.energy.29.082703.145619.

[4] S.J. Gerdemann, Wk O'Connor, D.C. Dahlin, L.R. Penner, H. Rush, Ex situ aqueous mineral carbonation, Environ. Sci. Technol. 41 (2007) 2587–2593, https://doi.org/10.1021/es0619253.

[5] P.B. Kelemen, J. Matter, E.E. Streit, J.F. Rudge, W.B. Curry, J. Blusztajn, Rates and mechanisms of mineral carbonation in peridotite: natural processes and recipes for enhanced, in situ CO_2 capture and storage, Annu. Rev. Earth. Planet. Sci. 39 (2011) 545–576, https://doi.org/10.1146/annurev-earth-092010-152509.

[6] A. Sanna, Mr Hall, M. Maroto-Valer, Post-processing pathways in carbon capture and storage by mineral carbonation (CCSM) towards the introduction of carbon neutral materials, Energy Environ. Sci. 5 (2012) 7781, https://doi.org/10.1039/c2ee03455g.

[7] S.Ó. Snæbjörnsdóttir, B. Sigfússon, C. Marieni, D. Goldberg, S.R. Gislason, E. H. Oelkers, Carbon dioxide storage through mineral carbonation, Nat. Rev. Earth Environ. 1 (2020) 90–102, https://doi.org/10.1038/s43017-019-0011-8.

[8] K.S. Lackner, C.H. Wendt, D.P. Butt, E.L. Joyce, D.H. Sharp, Carbon dioxide disposal in carbonate minerals, Energy 20 (1995) 1153–1170, https://doi.org/10.1016/0360-5442(95)00071-N.

[9] E. Benhelal, M.I. Rashid, M.S. Rayson, J.-D. Prigge, S. Molloy, G.F. Brent, A. Cote, M. Stockenhuber, E.M. Kennedy, Study on mineral carbonation of heat activated lizardite at pilot and laboratory scale, J. CO2 Util. 26 (2018) 230–238, https://doi.org/10.1016/j.jcou.2018.05.015.

[10] M.I. Rashid, E. Benhelal, F. Farhang, T.K. Oliver, M. Stockenhuber, E.M. Kennedy, Application of a concurrent grinding technique for two-stage aqueous mineral carbonation, J. CO2 Util. 42 (2020) 101347, https://doi.org/10.1016/j.jcou.2020.101347.

[11] M. Werner, S. Hariharan, M. Mazzotti, Flue gas CO_2 mineralization using thermally activated serpentine: from single- to double-step carbonation, Phys. Chem. Chem. Phys. 16 (2014) 24978–24993, https://doi.org/10.1039/C4CP02786H.

[12] F.W.K. Khudhur, J.M. Macdonald, A. Macente, L. Daly, The utilization of alkaline wastes in passive carbon capture and sequestration: Promises, challenges and environmental aspects, Sci. Total Environ. 823 (2022) 153553, https://doi.org/10.1016/j.scitotenv.2022.153553.

[13] J.M. Matter, P.B. Kelemen, Permanent storage of carbon dioxide in geological reservoirs by mineral carbonation, Nat. Geosci. 2 (2009) 837–841, https://doi.org/10.1038/ngeo683.

[14] M.T. Styles, A. Sanna, A.M. Lacinska, J. Naden, M. Maroto-Valer, The variation In composition of ultramafic rocks and the effect on their suitability for carbon dioxide sequestration by mineralization following acid leaching, Greenh. Gases: Sci. Technol. 4 (2014) 440–451, https://doi.org/10.1002/ghg.1405.

[15] P. Moita, E. Berrezueta, H. Abdoulghafour, M. Beltrame, J. Pedro, J. Mirão, C. Miguel, C. Galacho, F. Sitzia, P. Barrulas, J. Carneiro, Mineral carbonation of CO_2 in mafic plutonic rocks, II-laboratory experiments on early-phase supercritical CO_2-brine-rock interactions, Appl. Sci. 10 (2020) 5083, https://doi.org/10.3390/app10155083.

[16] A.H. Macdonald, W.S. Fyfe, Rate of serpentinization in seafloor environments, Tectonophysics 116 (1985) 123–135, https://doi.org/10.1016/0040-1951(85)90225-2.

[17] M. Andreani, L. Luquot, P. Gouze, M. Godard, E. Hoisé, B. Gibert, Experimental study of carbon sequestration reactions controlled by the percolation of CO_2-rich brine through peridotites, Environ. Sci. Technol. 43 (2009) 1226–1231, https://doi.org/10.1021/es8018429.

[18] H.E. King, O. Plümper, A. Putnis, Effect of secondary phase formation on the carbonation of olivine, Environ. Sci. Technol. 44 (2010) 6503–6509, https://doi.org/10.1021/es9038193.

[19] G. Gadikota, J. Matter, P. Kelemen, A.A. Park, Chemical and morphological changes during olivine carbonation for CO2 storage in the presence of NaCl and $NaHCO_3$, Phys. Chem. Chem. Phys. 16 (2014) 4679, https://doi.org/10.1039/c3cp54903h.

[20] A.K. Agrawal, A. Mehra, Dunite carbonation in batch-tubular reactor, Environ. Sci. Pollut. Res. 27 (2020) 31439–31445, https://doi.org/10.1007/s11356-020-09426-4.

[21] M.I. Rashid, E. benhelal, L. Anderberg, F. Farhang, T. Oliver, M.S. Rayson, M. Stockenhuber, Aqueous carbonation of peridotites for carbon utilisation: a critical review, Environ. Sci. Pollut. Res. 29 (2022) 75161–75183, https://doi.org/10.1007/s11356-022-23116-3.

[22] E.H. Oelkers, S.R. Gislason, P.B. Kelemen, Moving subsurface carbon mineral storage forward, Carbon Capture Sci. Technol. 6 (2023), https://doi.org/10.1016/j.ccst.2023.100098.

[23] A.L. Harrison, I.M. Power, G.M. Dipple, Accelerated carbonation of brucite in mine tailings for carbon sequestration, Environ. Sci. Technol. 47 (2013) 126–134, https://doi.org/10.1021/es3012854.

[24] J. Garnier, C. quantin, E. Guimarães, V.K. Garg, E.S. Martins, T. Becquer, Understanding the genesis of ultramafic soils and catena dynamics in Niquelândia, Brazil, Geoderma 151 (2009) 204–214, https://doi.org/10.1016/j.geoderma.2009.04.020.

[25] J. Kierczak, A. Pietranik, A. Pędziwiatr, Ultramafic geoecosystems as a natural source of Ni, Cr, and Co to the environment: a review, Sci. Total Environ. 755 (2021), https://doi.org/10.1016/j.scitotenv.2020.142620.

[26] W.F. McDonough, S. Sun, The composition of the Earth, Chem. Geol. 120 (1995) 223–253, https://doi.org/10.1016/0009-2541(94)00140-4.

[27] M. Sassi, S.N. Kerisit, Ni and Co incorporation in forsterite: a density functional theory study with hubbard correction, ACS Earth Space Chem. 8 (2024) 1027–1038, https://doi.org/10.1021/acsearthspacechem.3c00370.

[28] J.L. Hamilton, S. Wilson, B. Morgan, C.C. Turvey, D.J. Paterson, C. MacRae, J. McCutcheon, G. Southam, Nesquehonite sequesters transition metals and CO2 during accelerated carbon mineralisation, Int. J. Greenh. Gas. Control 55 (2016) 73–81, https://doi.org/10.1016/j.ijggc.2016.11.006.

[29] J.L. Hamilton, S. Wilson, B. Morgan, C.C. Turvey, D.J. Paterson, S.M. Jowitt, J. McCutcheon, G. Southam, Fate of transition metals during passive carbonation of ultramafic mine tailings via air capture with potential for metal resource recovery, Int. J. Greenh. Gas. Control 71 (2018) 155–167, https://doi.org/10.1016/j.ijggc.2018.02.008.

[30] Z. Iqbal Khan, K. Ahmad, T. Ahmad, A. Zafar, A.F. Alrefaei, A. Ashfaq, S. Akhtar, S. Mahpara, N. Mehmood, I. Ugulu, Evaluation of nickel toxicity and potential health implications of agriculturally diversely irrigated wheat crop varieties, Arab. J. Chem. 16 (2023) 104934, https://doi.org/10.1016/j.arabjc.2023.104934.

[31] World Health Organization, Nickel in drinking water: background document for development of WHO guidelines for drinking-water quality, 2021

[32] M. Cempel, G. Nikel, Nickel: A Review of Its Sources and Environmental Toxicology, Pol. J. Environ. Stud. 15 (2006) 375–382.

[33] R. Santos, A. van Audenaerde, Y. Chiang, R. Iacobescu, P. Knops, T. Van Gerven, Nickel extraction from olivine: effect of carbonation pre-treatment, Metals 5 (2015) 1620–1644, https://doi.org/10.3390/met5031620.

[34] F. Wang, D. Dreisinger, CO_2 Mineralization and Critical Battery Metals Recovery from Olivine and Nickel Laterites, in: 2023: pp. 63–74. ⟨https://doi.org/10.1007/978-3-031-22638-0_6⟩.

[35] S. Khan, M. Shoaib, L.K. Fiddes, O.B. Wani, E. R. Bobicki, CO_2 sequestration in ultramafic ores: impacts on the efficiency of nickel beneficiation, Green. Chem. 26 (2024) 1289–1296, https://doi.org/10.1039/D3GC02078A.

[36] P.M. Wojtulek, B. Schulz, R. Klemd, G. Gil, M. Dajek, K. Delura, The Central-Sudetic ophiolites – Remnants of the SSZ-type Devonian oceanic lithosphere in the

European part of the Variscan Orogen, Gondwana Res 105 (2022) 343–365, https://doi.org/10.1016/j.gr.2021.09.015.

[37] R. Kryza, C. Pin, The Central-Sudetic ophiolites (SW Poland): petrogenetic issues, geochronology and palaeotectonic implications, Gondwana Res 17 (2010) 292–305, https://doi.org/10.1016/j.gr.2009.11.001.

[38] J. Kierczak, B. Cieślik, A. Pietranik, K. Turniak, A. Lacinska, B. Keith, Mineral carbonation of ultramafic rocks from the Central Sudetic Ophiolite: an experimental approach, : Mineral. Spec. Pap., Mineral. Soc. Pol. 51 (2023) 73.

[39] P.B. Kelemen, J. Matter, In situ carbonation of peridotite for CO_2 storage, Proc. Natl. Acad. Sci. USA 105 (2008) 17295–17300, https://doi.org/10.1073/pnas.0805794105.

[40] Q.R.S. Miller, H.T. Schaef, J.P. Kaszuba, G. Gadikota, B.P. McGrail, K.M. Rosso, Quantitative review of olivine carbonation kinetics: reactivity trends, mechanistic insights, and research frontiers, Environ. Sci. Technol. Lett. 6 (2019) 431–442, https://doi.org/10.1021/acs.estlett.9b00301.

[41] A.M. Bremen, T. Strunge, H. Ostovari, H. Spütz, A. Mhamdi, P. Renforth, M. van der Spek, A. Bardow, A. Mitsos, Direct olivine carbonation: optimal process design for a low-emission and cost-efficient cement production, Ind. Eng. Chem. Res. 61 (2022) 13177–13190, https://doi.org/10.1021/acs.iecr.2c00984.

[42] S. Katre, P. Ochonma, H. Asgar, A.M. Nair, R. K, G. Gadikota, Mechanistic insights into the co-recovery of nickel and iron via integrated carbon mineralization of serpentinized peridotite by harnessing organic ligands, Phys. Chem. Chem. Phys. 26 (2024) 9264–9283, https://doi.org/10.1039/D3CP04996E.

[43] D.L. Parkhurst, C.A.J. Appelo. Description of input and examples for PHREEQC version 3: A computer program for speciation, batch-reaction, one-dimensional transport, and inverse geochemical calculations, 2013.

[44] C.S. Barnes, M. Koretsky, In Engineering and Chemical Thermodynamics, John Wiley & Sons, New York, 2004.

[45] K. Kularatne, O. Sissmann, F. Guyot, I. Martinez, Mineral carbonation of New Caledonian ultramafic mine slag: effect of glass and secondary silicates on the carbonation yield, Chem. Geol. 618 (2023) 121282, https://doi.org/10.1016/j.chemgeo.2022.121282.

[46] Ph Blanc, A. Lassin, P. Piantone, M. Azaroual, N. Jacquemet, A. Fabbri, E. C. Gaucher, Thermoddem: a geochemical database focused on low temperature water/rock interactions and waste materials, Appl. Geochem 27 (2012) 2107–2116, https://doi.org/10.1016/j.apgeochem.2012.06.002.

[47] J. Kierczak, A. Pędziwiatr, J. Waroszewski, M. Modelska, Mobility of Ni, Cr and Co in serpentine soils derived on various ultrabasic bedrocks under temperate climate, Geoderma 268 (2016) 78–91, https://doi.org/10.1016/j.geoderma.2016.01.025.

[48] B. Cieślik, J. Kierczak, A. Pietranik, Carbonate mineralization may reflect long-term evolution of ultramafic massifs: preliminary results from the Central-Sudetic Ophiolite (NE Bohemian Massif), in: XXII International Conference of Young Geologists, Smolenice, Slovakia, 2023, pp. 24–27.

[49] L. Gall, H.M. Williams, A.N. Halliday, A.C. Kerr, Nickel isotopic composition of the mantle, Geochim. Cosmochim. Acta 199 (2017) 196–209, https://doi.org/10.1016/j.gca.2016.11.016.

[50] H. Sato, Nickel content of basaltic magmas: identification of primary magmas and a measure of the degree of olivine fractionation, Lithos 10 (1977) 113–120, https://doi.org/10.1016/0024-4937(77)90037-8.

[51] S. Ishimaru, S. Arai, Nickel enrichment in mantle olivine beneath a volcanic front, Contrib. Mineral. Pet. 156 (2008) 119–131, https://doi.org/10.1007/s00410-007-0277-6.

[52] O. Fesharaki, E. García-Romero, J. Cuevas-González, N. López-Martínez, Clay mineral genesis and chemical evolution in the Miocene sediments of Somosaguas, Madrid Basin, Spain, Clay Min. 42 (2007) 187–201, https://doi.org/10.1180/claymin.2007.042.2.05.

[53] Y. Liu, Mechanism for the dissolution of olivine series minerals in acidic solutions, Am. Miner. 91 (2006) 455–458, https://doi.org/10.2138/am.2006.2077.

[54] A. Sanna, M. Uibu, G. Caramanna, R. Kuusik, M.M. Maroto-Valer, A review of mineral carbonation technologies to sequester CO_2, Chem. Soc. Rev. 43 (2014) 8049–8080, https://doi.org/10.1039/C4CS00035H.

[55] E.H. Oelkers, J. Declercq, G.D. Saldi, S.R. Gislason, J. Schott, Olivine dissolution rates: a critical review, Chem. Geol. 500 (2018) 1–19, https://doi.org/10.1016/j.chemgeo.2018.10.008.

[56] S. Stokreef, F. Sadri, A. Stokreef, A. Ghahreman, Mineral carbonation of ultramafic tailings: a review of reaction mechanisms and kinetics, industry case studies, and modelling, Clean. Eng. Technol. 8 (2022), https://doi.org/10.1016/j.clet.2022.100491.

[57] Y. Ji, D. Madhav, V. Vandeginste, Kinetics of enhanced magnesium carbonate formation for CO_2 storage via mineralization at 200 °C, Int. J. Greenh. Gas. Control 121 (2022) 103777, https://doi.org/10.1016/j.ijggc.2022.103777.

[58] V. Bermanec, G. Sijaric, G. Kniewald, J.A. Mandarino, Gaspéite and associated Ni-rich minerals from veins in altered ultrabasic Rocks from Dubostica, Bosnia and Herzegovina, Can. Miner. 38 (2000) 1371–1376, https://doi.org/10.2113/gscanmin.38.6.1371.

[59] A. Villegas-Jiménez, A. Mucci, O.S. Pokrovsky, J. Schott, Acid−base behavior of the gaspeite ($NiCO_3$ (s)) surface in NaCl solutions, Langmuir 26 (2010) 12626–12639, https://doi.org/10.1021/la9041088.

[60] O.S. Pokrovsky, J. Schott, Surface chemistry and dissolution kinetics of divalent metal carbonates, Environ. Sci. Technol. 36 (2002) 426–432, https://doi.org/10.1021/es010925u.

[61] H. Béarat, Mj McKelvy, A.V.G. Chizmeshya, D. Gormley, R. Nunez, R.W. Carpenter, K. Squires, G.H. Wolf, Carbon sequestration via aqueous olivine mineral carbonation: role of passivating layer formation, Environ. Sci. Technol. 40 (2006) 4802–4808, https://doi.org/10.1021/es0523340.

[62] O. Rahmani, J. Highfield, R. Junin, M. Tyrer, A. Pour, Experimental investigation and simplistic geochemical modeling of CO_2 mineral carbonation using the Mount Tawai peridotite, Molecules 21 (2016) 353, https://doi.org/10.3390/molecules21030353.

[63] A.M. Lacinska, Mt styles, K. Bateman, M. Hall, P.D. Brown, An experimental study of the carbonation of serpentinite and partially serpentinised peridotites, Front. Earth Sci. 5 (2017), https://doi.org/10.3389/feart.2017.00037.

[64] E.H. Oelkers, S.R. Gislason, J. Matter, Mineral carbonation of CO_2, Elements 4 (2008) 333–337, https://doi.org/10.2113/gselements.4.5.333.

[65] N.C. Johnson, B. Thomas, K. Maher, R.J. Rosenbauer, D. Bird, G.E. Brown, Olivine dissolution and carbonation under conditions relevant for in situ carbon storage, Chem. Geol. 373 (2014) 93–105, https://doi.org/10.1016/j.chemgeo.2014.02.026.

[66] S. Yadav, A. Mehra, A review on ex situ mineral carbonation, Environ. Sci. Pollut. Res. 28 (2021) 12202–12231, https://doi.org/10.1007/s11356-020-12049-4.

[67] S. Monico, M. Cantaluppi, V. Diella, G.D. Gatta, I. Adamo, P. Fumagalli, N. Marinoni, Similarities and differences among selected gemmological varieties of chalcedony: chemistry, mineralogy and microstructure, Mineral. Mag. 88 (2024) 136–146, https://doi.org/10.1180/mgm.2023.92.

[68] P.J. Heaney, A proposed mechanism for the growth of chalcedony, Contrib. Mineral. Pet. 115 (1993) 66–74, https://doi.org/10.1007/BF00712979.

[69] B.G. Haile, H. Hellevang, P. Aagaard, J. Jahren, Experimental nucleation and growth of smectite and chlorite coatings on clean feldspar and quartz grain surfaces, Mar. Pet. Geol. 68 (2015) 664–674, https://doi.org/10.1016/j.marpetgeo.2015.02.006.

[70] A.W. Priestas, S.W. wise, Distribution and origin of authigenic smectite clays in Cape Roberts Project Core 3, Victoria Land Basin, Antarctica (2007), https://doi.org/10.3133/ofr20071047SRP057.

[71] H. Ren, J. Cheng, H. Fang, F. Zhong, C. Chen, L. Lin, Y. Luo, C. Au, L. Jiang, X. Lin, Phyllosilicate-derived Ni catalysts with small nanoparticle size and strong metal-support interaction for efficient and robust decomposition of ammonia, Appl. Catal. A Gen. 664 (2023) 119344, https://doi.org/10.1016/j.apcata.2023.119344.

[72] J.-H. Lee, E.-B. Cho, High hydrothermal stability of mesoporous Ni-phyllosilicate spherical particles, Appl. Surf. Sci. 590 (2022) 153114, https://doi.org/10.1016/j.apsusc.2022.153114.

[73] Y. Zhang, Q. Liu, Nickel phyllosilicate derived Ni/SiO_2 catalysts for CO_2 methanation: Identifying effect of silanol group concentration, J. CO2 Util. 50 (2021) 101587, https://doi.org/10.1016/j.jcou.2021.101587.

[74] C.R.M. Butt, D. Cluzel, Nickel laterite ore deposits: weathered serpentinites, Elements 9 (2013) 123–128, https://doi.org/10.2113/gselements.9.2.123.

[75] C. Villanova-de-Benavent, F. Nieto, C. Viti, J.A. Proenza, S. Galí, J. Roqué-Rosell, Ni-phyllosilicates (garnierites) from the Falcondo Ni-laterite deposit (Dominican Republic): mineralogy, nanotextures, and formation mechanisms by HRTEM and AEM, Am. Miner. 101 (2016) 1460–1473, https://doi.org/10.2138/am-2016-5518.

[76] M. Ulrich, M. Muñoz, S. Guillot, M. Cathelineau, C. Picard, B. Quesnel, P. Boulvais, C. Couteau, Dissolution–precipitation processes governing the carbonation and silicification of the serpentinite sole of the New Caledonia ophiolite, Contrib. Mineral. Pet. 167 (2014) 1–19, https://doi.org/10.1007/s00410-013-0952-8.

[77] A.S. Majumdar, H.E. King, T. John, C. Kusebauch, A. Putnis, Pseudomorphic replacement of diopside during interaction with $(Ni,Mg)Cl_2$ aqueous solutions: implications for the Ni-enrichment mechanism in talc- and serpentine-type phases, Chem. Geol. 380 (2014) 27–40, https://doi.org/10.1016/j.chemgeo.2014.04.016.

[78] R.J.M.J. Vogels, J.T. Kloprogge, J.W. Geus, Synthesis and characterization of saponite clays, Am. Miner. 90 (2005) 931–944, https://doi.org/10.2138/am.2005.1616.

[79] F. Wang, D. Dreisinger, Carbon mineralization with concurrent critical metal recovery from olivine, Proc. Natl. Acad. Sci. USA 119 (2022), https://doi.org/10.1073/pnas.2203937119.

[80] C. Villanova-de-Benavent, T. Jawhari, J. Roqué-Rosell, S. Galí, J.A. Proenza, Ni-bearing phyllosilicates ("garnierites"): new insights from thermal analysis, μRaman and IR spectroscopy, Appl. Clay Sci. 175 (2019) 47–66, https://doi.org/10.1016/j.clay.2019.03.036.

[81] F. Montserrat, P. Renforth, J. Hartmann, M. Leermakers, P. Knops, F.J.R. Meysman, Olivine dissolution in seawater: implications for CO 2 sequestration through enhanced weathering in coastal environments, Environ. Sci. Technol. 51 (2017) 3960–3972, https://doi.org/10.1021/acs.est.6b05942.

[82] H.H. Namaghi, G.H. Karami, S. Saadat, A study on chemical properties of groundwater and soil in ophiolitic rocks in Firuzabad, east of Shahrood, Iran: with emphasis to heavy metal contamination, Environ. Monit. Assess. 174 (2011) 573–583, https://doi.org/10.1007/s10661-010-1479-3.

[83] A. Langone, I. Baneschi, C. Boschi, A. Dini, M. Guidi, A. Cavallo, Serpentinite-water interaction and chromium(VI) release in spring waters: examples from Tuscan ophiolites, Ofioliti 38 (2013) 41–57, https://doi.org/10.4454/ofioliti.v38i1.415.

[84] N. Voutsis, E. Kelepertzis, E. Tziritis, A. Kelepertsis, Assessing the hydrogeochemistry of groundwaters in ophiolite areas of Euboea Island, Greece, using multivariate statistical methods, J. Geochem. Explor. 159 (2015) 79–92, https://doi.org/10.1016/j.gexplo.2015.08.007.